Nuclear Instruments and Methods in Physics Research B 84 (1994) 323–330
North-Holland

NIM B
Beam Interactions with Materials & Atoms

Amorphization of Al_2O_3 by ion induced density reduction

E.D. Specht *, D.A. Walko + and S.J. Zinkle
Metals and Ceramics Division, Oak Ridge National Laboratory Oak Ridge, Tennessee 37831-6118, USA

Received 28 April 1993 and in revised form 17 July 1993

Al_2O_3 at room temperature amorphizes at an anomalously high ion implantation dose, corresponding to hundreds of displacements per atom (dpa). We have performed X-ray reflectometry and Monte Carlo simulations, which show that amorphization near the surface is preceded by a progressive reduction in density caused by high-energy-transfer elastic collisions which knock Al and O atoms deeper into the crystal. Electron microscopy shows that the reduction in density is at least partially accommodated by void formation. We propose that the accumulation of these and other low-density defects such as vacancy clusters and nuclei of amorphous and lower-density crystalline phases of Al_2O_3 may serve as a mechanism for high-dose amorphization.

1. Introduction

Many crystalline materials, including semiconductors [1], insulators [2,3], and some intermetallic compounds [4] can be amorphized by ion irradiation. For ions and targets of relatively high atomic number and for relatively low ion beam energies, the energy lost by the ion is concentrated in a thermal spike [5] which can lead to amorphization along a single ion cascade by the melting of a small region followed by rapid cooling. In this paper we are concerned with relatively light atoms and high energies, where amorphization follows an accumulation of independent atomic displacements rather than a collective, thermal process. As ions displace atoms from lattice sites to create vacancy–interstitial pairs and other associated defects, one of two things may occur. In some crystals, an equilibrium defect concentration is reached, where further ion bombardment stimulates the recombination of defects at the same rate as their production. In other cases, and especially at low temperatures, damage proceeds to amorphization. In most cases, the damage to the lattice saturates at a dose on the order of 0.1 to 1 dpa.

For Al_2O_3, ZrO_2, MgO, and WC amorphization follows a different pattern [2,6–8]. At cryogenic temperatures these materials behave as just described, amorphizing at a dose of a few dpa. Amorphization at room temperature, however, can require a dose on the order of 100 dpa. The mechanism for amorphization at this dose is not clearly understood. We address the possible origin of this anomalously high amorphization threshold.

We consider ion energies that produce a buried layer of the incident species at the ion end of range (eor). The resulting change in chemical composition complicates damage to this layer, which is strongly dependent on factors such as the solubility and size of the implanted atom [3,9]. Therefore we focus on the midrange region between the eor and surface; here the ions create damage but are not deposited. Simulations (described in section 3) show that 90% of the ions implanted in our samples fall in an eor at a depth of 30 to 130 nm.

Processes that may contribute to amorphization include chemical effects, defect formation, and density changes. The chemistry of implanted ions is a critical factor in amorphization of the eor: in particular the amorphization threshold of Al_2O_3 is much higher for implanted species which occupy substitutional sites on the Al_2O_3 lattice [3,9,10]. Chemical effects may occur in the midrange as well. While thermal diffusion is negligible at the implantation temperatures at which amorphization occurs, enhanced transport of implanted species may result from the defects introduced by implantation, leading to chemical effects in the midrange. For example, amorphization induced by chemical effects in the endrange may speed diffusion of the implanted species, propagating amorphization through the midrange. Even the relatively low concentrations of implanted ions which come to rest in the midrange with no diffusion may lead to amorphization by inhibiting damage recovery mechanisms.

* Corresponding author.
+ Current address: Department of Physics, University of Illinois, Urbana, IL 61801-3080, USA.

SSDI 0168-583X(93)E0687-C

Amorphization can also result from the accumulation of atomic displacements. It has been shown that low temperature Si, for example, amorphizes when ~ 10% of the atoms are displaced from lattice sites [11,12]. Burnett and Page [2] have observed that ionic compounds are more resistant to amorphization, suggesting that amorphization occurs in these materials when a critical density ρ_{Ecrit} of energy is deposited as substrate lattice damage (ρ_{Ecrit} ~ 7 keV per substrate atom, enough to create ~ 160 displacements). Such a high ρ_{Ecrit} implies substantial damage recovery. Bull [13] applies a simple kinetic model to high-dose amorphization, assuming a thermally activated process for the annealing of atomic displacements. He finds that ρ_{Ecrit} depends only weakly on temperature, ruling out a simple thermal recovery mechanism.

Atomic displacements account for amorphization near 1 dpa, and chemical effects are responsible for amorphization which occurs at a relatively low dose for a particular implanted element. We propose a third mechanism for high-dose amorphization. High-energy-transfer collisions will knock some host atoms deep into the host, leaving a shallow vacancy and a deep interstitial. While nearby vacancies and interstitials recombine, those that are widely separated cannot recombine, and will accumulate. A characteristic damage morphology, attributed to this separation of vacancies and interstitials, has been observed in ion-implanted silicon [14]. In the absence of recovery mechanisms, density will decrease in the midrange and increase in the eor. A critically low (or high) density may lead to amorphization. Amorphization occurs at a high dose because of the low cross-section for high-energy-transfer collisions.

In this paper we report measurements of the density changes induced in the crystalline state by ion implantation at doses below the amorphization threshold. Cr-implanted Al_2O_3 was used, as it as been shown to amorphize at extremely high doses [7]. X-ray reflectivity measurements are used to measure the extent to which the density of the midrange is reduced by ion bombardment. Monte Carlo calculations show that this reduction results from midrange substrate atoms being knocked deeper into the crystal. We discuss how this excess of vacancies over interstitials may lead to amorphization.

2. Experimental results

2.1. Implantation

High purity [0001] oriented α-Al_2O_3 (sapphire) single crystals with an optical grade polish were annealed in air at 1775 K for 5 days, then implanted with 160 keV Cr^+ ions at room temperature. To avoid ion channeling, the incident beam direction was ~ 5° off the specimen normal. Rutherford backscattering [7], indentation [7,15], and glancing angle X-ray diffraction [16] measurements have been reported for these samples, showing that amorphization occurs in the eor at a fluence of 1×10^{17} ions/cm^2, growing with increasing fluence and reaching the surface at 6×10^{17} ions/cm^2.

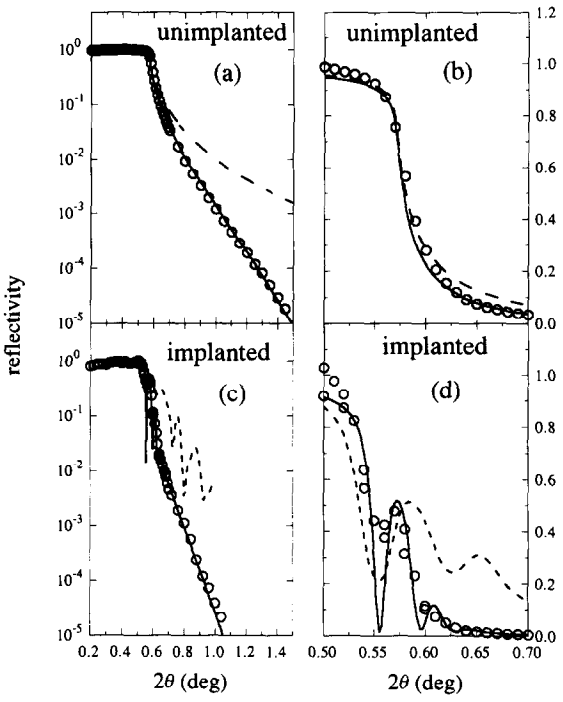

Fig. 1. X-ray reflectivity of Al_2O_3, unimplanted ((a) and (b)) and implanted with 1×10^{17} Cr^+/cm^2. Panels (a) and (c): semilog scale. Panels (b) and (d): detail on a linear scale. Measured reflectivity: (○). Solid and dashed lines are calculated from the corresponding densities in Fig. 2 as described in the text.

2.2. X-ray reflectivity

The X-ray reflectivities were measured as described in detail by Cowley and Ryan [17]. Briefly, a triple-axis system was used where a Ge(111) crystal selects the K_α fluorescence from a rotating Cu anode X-ray source, a 0.5 mm slit before the sample selects the $K_{\alpha 1}$ component, and another Ge(111) crystal selects Cu $K_{\alpha 1}$ X-rays reflected at each scattering angle 2θ. Reflected intensity is integrated over a rocking curve for each value of 2θ. Shown in Fig. 1 are the reflectivities of Al_2O_3 crystals, unimplanted and implanted with 1×10^{17} Cr^+/cm^2, which corresponds to a dose of 54 dpa in the midrange, as derived from Monte Carlo calculations described in section 3. For the unimplanted sample (Figs. 1a and 1b), reflectivity is close to unity up to the

critical angle θ_c, which is proportional to the square root of the electron density; at higher angles reflectivity falls rapidly. After implantation (Figs. 1c and 1d), reflected intensity begins to fall when $\theta < \theta_c$. For θ just below θ_c, the reduced density of the midrange is insufficient for the total reflection of X-rays, which *are* totally reflected by the denser eor; absorption by implanted Cr atoms accounts for the reduced intensity. Increased scattering is observed near $2\theta = 0.57°$ due to interference between X-rays reflected from the surface and from the interface between low and high density material. Higher diffraction orders are not visible because this interface is diffuse.

A quantitative model for the depth profile of the density can be developed by choosing a functional form based on the qualitative features just described and varying the parameters to give a least-squares fit to the reflectivity. The density profile was approximated by 302 uniform layers: infinitely thick air and bulk Al_2O_3 layers separated by 300 layers, each $t = 1$ nm thick. Reflectivity was calculated from the electron density and X-ray absorption using the theory of Parratt [18]. The reflectivity of the unimplanted sample is modeled using a single Gaussian-smeared step [19],

$$\rho(z) = \frac{\rho_{\text{bulk}}}{2}\left[1 + \text{erf}\frac{z}{\sqrt{2}\sigma}\right], \qquad (1)$$

where ρ is the density, z is the depth, σ is the rms surface roughness, and erf is the error function [20]. The incident X-ray power is a free parameter for all fits. As shown in Figs. 1a and 1b (solid lines), we obtain an excellent fit with $\sigma = 2.18$ nm and $\rho_{\text{bulk}} = 3.983$ g/cm^3, agreeing well with the conventional Al_2O_3 X-ray density of 3.985 g/cm^3 [21].

For the implanted samples, the distribution of Cr atoms is approximated by a Gaussian. While the total absorption is taken to match the Cr^+ dose, we find the electron density in the eor to be less than that of Al_2O_3 plus implanted Cr. From the dashed curves in Figs. 1c, 1d, and 2b, we see that such a high density would lead to much higher reflectivity above the bulk critical angle of 0.56° than we have observed. Mathematically, we account for this by reducing the electron density contributed by the Cr. Physically, we conclude that the eor has expanded. We model the Al_2O_3 density by generalizing Eq. (1) to include two Gaussian-smeared steps, one at $z = 0$ from density 0 to $d\rho_{\text{bulk}}$ with width σ_s, the other at $z = z_d$ from density $d\rho_{\text{bulk}}$ to ρ_{bulk} with width σ_d:

$$\rho_{Al_2O_3}(z) = \frac{\rho_{\text{bulk}}}{2}\left[1 + \text{erf}\frac{z}{\sqrt{2}\sigma_s}\right] \times\left[d + (1-d)\,\text{erf}\frac{z - z_d}{\sqrt{2}\sigma_d}\right]. \qquad (2)$$

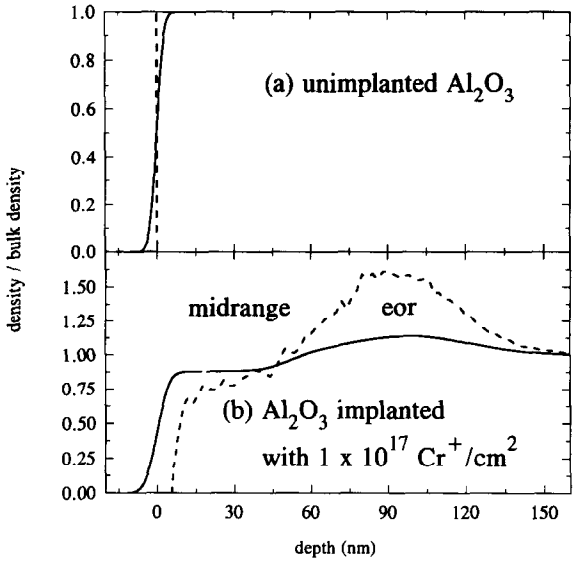

Fig. 2. Density profiles: (a) Unimplanted Al_2O_3. Dashed line is calculated for a sharp interface. Solid line is the best fit of Eq. (1) to the measured reflectivity. (b) Ion-implanted Al_2O_3. Dashed line is calculated from a Monte Carlo simulation. Solid line is the best fit of Eq. (2) to the measured reflectivity.

For the sample implanted with 1×10^{17} Cr^+/cm^2, the best fit (solid line in Fig. 2b) is obtained for surface density $d = 0.880$ of the bulk value, surface roughness $\sigma_s = 3.7$ nm, interface roughness $\sigma_d = 8.3$ nm, interface depth $z_d = 52$ nm, and a Gaussian Cr layer which is 98 nm deep and 55.3 nm full width at half maximum. The

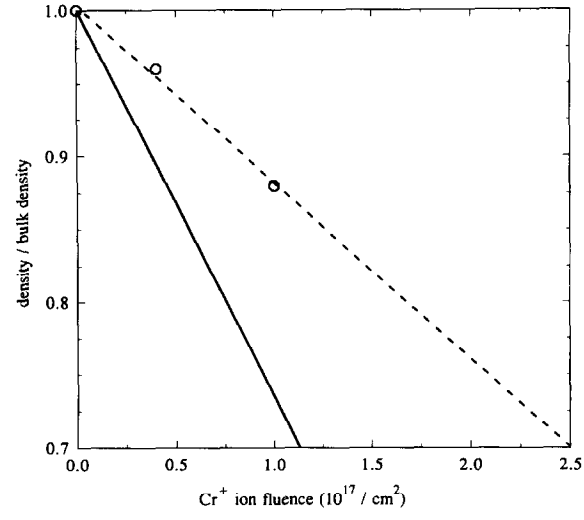

Fig. 3. (○): surface density of Al_2O_3 implanted with 160 keV Cr^+ ions, measured using X-ray reflectivity. The dashed line is a guide to the eye. Solid line: surface density from Monte Carlo simulation.

best-fit maximum density of the implanted Cr layer is 0.139 of the bulk Al_2O_3 density. The width and depth of the implanted Cr distribution are close to those calculated in the simulation described below. The agreement with the observed reflectivity is good (solid lines in Figs. 1c and 1d); the sharpest interference features are diminished by an experimental resolution of $\sim 0.01°$.

For another sample implanted with only 4×10^{16} Cr^+/cm^2, the effects of implantation are weaker, so the reflectivity is fit using the parameters determined from the 1×10^{17} Cr^+/cm^2 sample, varying only d (0.961), σ_s (2.8 nm), and the maximum density of the Cr layer (0.125 of bulk). Surface density versus dose is indicated by the circles in Fig. 3.

2.3. Electron microscopy

Implanted samples were cut in half and the two pieces were glued face-to-face, sectioned, and ion milled to obtain cross-section transmission electron microscopy (TEM) specimens. Fig. 4 shows a bright field TEM image of the 4×10^{16} Cr^+/cm^2 sample. A dense array of dislocation loops and network is present in the eor between the depths of 65 and 230 nm. The midrange region between the surface and a depth of 60

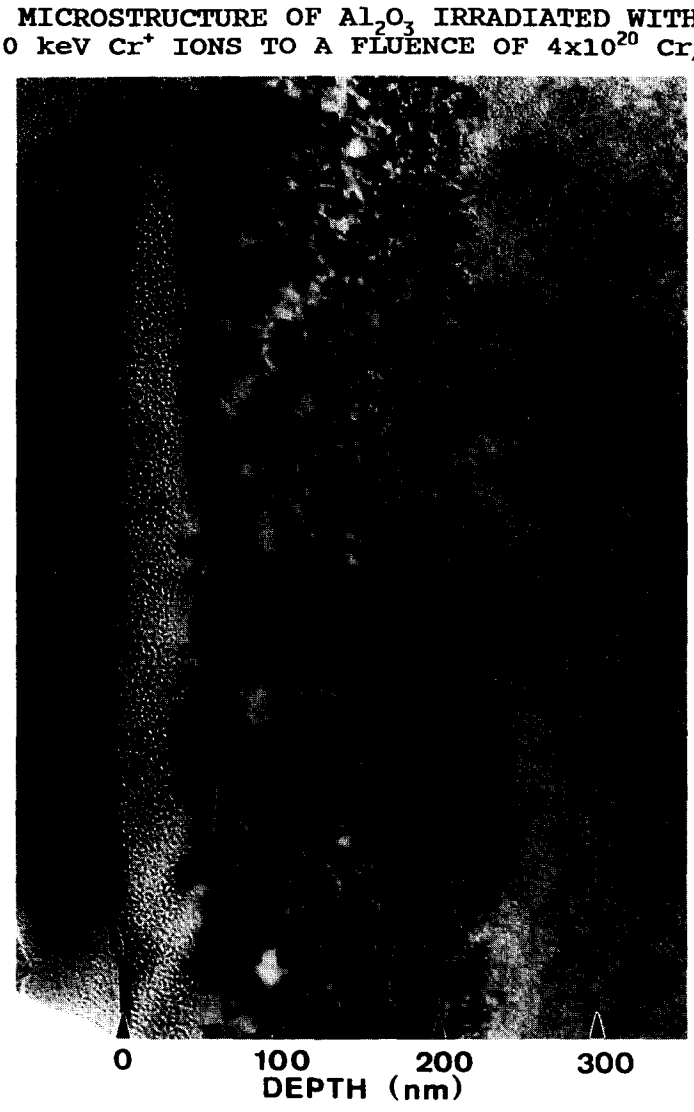

Fig. 4. Cross-section transmission electron micrograph showing the microstructure observed in Al_2O_3 after implantation with 4×10^{16} Cr^+/cm^2. The beam normal was near $[2\bar{1}\bar{1}0]$ The photo was taken in an underfocussed condition to enhance the visibility of the midrange cavities.

nm, on the other hand, is free of visible dislocations and contains a high density ($\sim 5 \times 10^{23}/m^3$) of small ($\sim 2$ nm) features which exhibit contrast consistent with that of voids. The volume fraction associated with these voids is only $\sim 0.2\%$, much smaller than the midrange density reduction of 4% determined from the X-ray reflectometry measurements. Electron microdiffraction analysis of the midrange and eor showed no significant change ($< 1\%$) in the lattice parameter compared to the undamaged Al_2O_3 substrate. There was no evidence for the formation of amorphous zones in either the midrange or eor regions. Similar microstructural features were observed in the higher dose sample irradiated with 1×10^{17} Cr^+/cm^2 (Fig. 5). The observed extent of the damaged region in both the lower and higher dose specimens was 230 nm, which is approximately 65% deeper than the 140 nm damage range calculated by TRIM. The experimental damage

Fig. 5. Cross-section transmission electron micrograph showing the depth-dependent microstructure of Al_2O_3 after implantation with 1×10^{17} Cr^+/cm^2, taken in an underfocussed condition, with beam normal near $[2\bar{1}\bar{1}0]$.

range determined by TEM is in agreement with the damage range deduced from the X-ray reflectivity data. The discrepancy between the observed and calculated damage range is generally attributed to errors in the electronic stopping powers used in the calculations. The surface roughness of the irradiated samples could be directly measured in the cross-section TEM specimens by examination of the interface between the glue and the specimen surface. The surface roughness observed by TEM in both the lower and higher dose samples was very small, in agreement with the fitted parameters from the X-ray reflectivity data.

What causes the reduction in midrange density? Hioki et al. have shown that the vacancy–interstitial pairs produced by ion implantation of Al_2O_3 at cryogenic temperatures lead to a lattice expansion of $\sim 2\%$ at doses of ~ 0.1 dpa [22]. However, glancing angle X-ray Bragg diffraction measurements on our room temperature samples have shown that the unit cell volume of the Al_2O_3 lattice is expanded by only 0.3% [16], a minor contribution to the density change. Thus we attribute the density reduction to a surplus of vacancies over interstitials in the lattice, rather than a lattice expansion. Surplus vacancies would be left if interstitial atoms formed new planes in the crystal; however, this may be ruled out because dislocation loops, which must surround the new planes, are absent in the midrange (Fig. 4). The only plausible cause of the density reduction is the high-energy-transfer collisions which knock Al and O atoms deep into the crystal and give rise to excess shallow vacancies and deep interstitials.

3. Monte Carlo simulations

Monte Carlo simulations of ion trajectories were used to calculate the effects of collisions. We have applied the TRIM89 code [23], which tracks the paths of implanted ions and the substrate atoms with which they collide, including the effects of electronic energy loss. The simulation takes into account neither the crystalline structure of the substrate nor the effects of ion beam modification: each ion and atom is assumed to pass through undamaged but amorphous Al_2O_3; thus all effects are linear in ion dose. The change in density is caused predominantly by high-energy-transfer collisions, for which the cross sections are accurately known [24], and depend little on crystal structure. In contrast, dpa values depend on the energy of target atom displacement. Displacement energies determined for crystalline Al_2O_3 are used (18 eV for Al and 72 eV for O) [25], likely leading to an underestimate of atomic displacements. Thus we expect TRIM89 to provide an accurate simulation of the density effects of ion bombardment, with large discrepancies due only to recovery processes, which are not included in the simulation.

The dashed line in Fig. 2b indicates the results of the simulation of 1×10^{17} Cr^+/cm^2 implantation. The uppermost 5 nm are gone, with 75% of the atoms sputtered off and 25% knocked into the substrate. Because translation of the sample does not alter its reflectivity, no effect of this shift of the surface is apparent in the reflectivity. The next 50 nm are reduced in density by collisions which knock atoms deeper into the substrate. The simulation (dashed line in Fig. 2b) predicts a relative excess of vacancies of $\sim 10^{-3}$ corresponding to a density of 0.71 of bulk at the surface, over twice the decrease deduced from X-ray reflectivity (solid line in Fig. 2b), which indicates a density of 0.88. The largest discrepancy seen in Fig. 2b is in the region where the implanted Cr ions and the knocked-on aluminum and oxygen atoms pile up. As mentioned above, our reflectivity results rule out such a high density. We will concentrate, however, on the region nearer the surface.

4. Discussion

Fig. 3 shows that the measured density at the surface decreases at half the rate predicted by the Monte Carlo simulation. We attribute the difference to recovery processes. While diffusion of vacancies and interstitials is negligible both at room temperature without ion implantation [26,27], and at lower temperatures under implantation [9,22,28], we propose that Al_2O_3 samples implanted at room temperature exhibit a high amorphization threshold because a local equilibrium is established where vacancies and interstitials recombine at the same rate that they are produced. As vacancies and interstitials continue to recombine locally, the small fraction of excess vacancies produced in the midrange accumulates. Comparison of experiment and simulation shows this combination of thermal and ion-induced diffusion leads to the recombination of some of the more widely separated pairs as well. The progressive reduction in density points toward a competing mechanism which converts excess vacancies to a more stable defect. Such a defect might be a microvoid, a region of Al_2O_3 which is amorphous or of a less dense crystalline phase, or a cluster of vacancies. The density reduction that is directly attributable to the voids in the lower-dose sample shown in Fig. 4 is only $\sim 0.2\%$, which is much less than the midrange density change of 4% measured by X-ray reflectometry.

Amorphization in ion-implanted ceramics generally begins in the eor, progressing to the surface [3]. Table 1 lists the critical fluences observed for amorphization of the surface of Al_2O_3 by implantation with several ions. We have used Monte Carlo calculations as de-

Table 1
Number of atomic displacements (dose) and relative density change ($\Delta\rho/\rho$) at the observed thresholds for surface amorphization of Al_2O_3 at room temperature. The dose is based on a Monte Carlo calculation with no recovery; density change includes 50% recovery as reported in this paper

Ion	Energy [keV]	Fluence [10^{17} ions/cm^2]	Dose [dpa]	$\Delta\rho/\rho$
Co	400	3–5 (ref. [8])	230–380	0.19–0.32
Cr	160	3–6 (ref. [7])	160–320	0.40–0.80
Ti	300	3–5 (ref. [2])	110–180	0.18–0.31
Y	300	0.8–1 (ref. [2])	60–80	0.19–0.24

scribed above to convert these fluences to both a dpa dose and a density decrease. The density decrease at which amorphization occurs is the same for three of the ions (Co, Ti, and Y), which suggests that it is the density change which causes amorphization. We note, however, that the exception is Cr, which is the only atom which can substitute for Al in Al_2O_3 with no second phase formation. The higher critical density change for Cr suggests that second phase formation may be an important factor in amorphization. Monte Carlo calculations indicate that negligible concentrations of implanted ions come to rest near the surface, but ion bombardment produces anomalously high diffusion rates, as demonstrated by the partial recovery of the density. Thus we cannot rule out large implanted ion concentrations near the surface.

Chemical effects could be definitively ruled out by the stoichiometric co-implantation of Al and O ions, as described by White et al. [29]. According to Monte Carlo calculations, these lighter ions require fluences of $\sim 10^{19}$/cm^2 to cause critical density changes. Alternatively, chemical effects can be avoided using higher energy implantation in which the eor and midrange are widely separated. However, more energetic ions have a lower cross section for high-energy-transfer collisions, so again much higher ion fluences would be required. Along with higher-fluence sources, efficient sample cooling would be needed, as discussed by Bull [13]. Further evidence as to the amorphization mechanism might be obtained from the structure of the amorphous phase. As pointed out by Bull [13], amorphization by a chemical mechanism may give rise to a distinctive amorphous structure. When amorphization is due to density reduction, we would expect little dependence of either the critical density for amorphization or the structure of the amorphous phase on the implanted element.

If density reduction is indeed the mechanism for high-dose amorphization, then there would be *no limit* to the lattice damage which could be accommodated by Al_2O_3 at room temperature. Because lighter ions produce more lattice displacements relative to high-energy-transfer collisions, light-ion implantation could distinguish between density reduction and critical energy density amorphization mechanisms. For example, a fluence of 10^{19} Ne$^+$/cm^2 is calculated to produce a density reduction of just 10% (well below the amorphization threshold) and deposit 86 keV per substrate atom in lattice damage (well above threshold).

Local atomic displacements lead to amorphization at sufficiently low temperatures, but vacancy–interstitial recombination leads to an equilibrium concentration of vacancy–interstitial pairs for Al_2O_3 at room temperature. Chemical effects will lead to amorphization in many cases, but this mechanism is less effective in the midrange and for more soluble atoms such as Cr; it will certainly be absent for self-implantation. We have shown that high-energy-transfer collisions lead to a progressive density decrease in the midrange. We propose that in the absence of competing mechanisms this density decrease will lead to amorphization. We have focused on the midrange because study of the eor is complicated by the presence of implanted ions, but a complementary mechanism may operate in the eor: amorphization results from an increase in density brought about by the combination of implanted ions and knocked-on atoms. The partial recovery of the density from the values predicted by Monte Carlo calculations suggests that single vacancies will recombine with displaced interstitials during room temperature implantation; we conclude that the remaining vacancies condense into a more stable form. Some voids have been observed, and other vacancies may form submicroscopic vacancy clusters or small nuclei of amorphous or lower-density phases of crystalline Al_2O_3. As may be seen from Table 1, amorphization occurs when the calculated density approaches that of amorphous Al_2O_3 ($\Delta\rho/\rho = 0.3$) [30]. The defective crystalline Al_2O_3 may become unstable as its density approaches that of the amorphous phase.

Acknowledgements

We are grateful to M. O'Hern, L. Romana, and J.E. Pawel for assistance in sample preparation and to O.W. Holland, D.L. Joslin, C.J. McHargue, R.A. McKee, D.F. Pedraza, C.J. Sparks, and F.J. Walker for helpful discussions. This work was sponsored by the Division of Materials Sciences and by the Office of Fusion Energy, U.S. Department of Energy, under contract DE-AC05-84OR21400 with Martin Marietta Energy Systems, Inc.

References

[1] E. Glaser, G. Götz, N. Sobolev and W. Wesch, Phys. Status Solidi A 69 (1982) 603.

[2] P.J. Burnett and T.F. Page, Radiat. Eff. 97 (1986) 283.
[3] C.W. White, C.J. McHargue, P.S. Sklad, L.A. Boatner and G.C. Farlow, Mater. Sci. Rep. 4 (1989) 41.
[4] J.L. Brimhall and E.P. Simonen, Nucl. Instr. and Meth. B 16 (1986) 187.
[5] P. Sigmund, Appl. Phys. Lett. 25 (1974) 169.
[6] P.J. Burnett and T.F. Page, J. Mater. Sci. 20 (1985) 4624.
[7] M.E. O'Hern, L.J. Romana, C.J. McHargue, J.C. McCallum and C.W. White, Proc. 15th Symp. on Radiation Effects on Materials, ed. R. Stoller (ASTM, Philadelphia, 1992) p. 740.
[8] S. Noda, H. Doi and O. Kamigaito, J. Mater. Res. 4 (1989) 671.
[9] C.J. McHargue, G.C. Farlow, G.M. Begun, J.M. Williams, C.W. White, B.R. Appleton, P.S. Sklad and P. Angelini, Nucl. Instr. and Meth. B 16 (1986) 212.
[10] C.J. McHargue, G.C. Farlow, C.W. White, J.M. Williams, B.R. Appleton and H. Naramoto, Mater. Sci. 69 (1985) 123.
[11] P.J. Burnett and T.F. Page, J. Mater. Sci. 19 (1984) 845.
[12] L.A. Christel, J.F. Gibbons and T.W. Sigmon, J. Appl. Phys. 52 (1981) 7143.
[13] S.J. Bull, J. Mater. Sci. 26 (1991) 3086.
[14] O.W. Holland and C.W. White, Nucl. Instr. and Meth. B 59/60 (1991) 353.
[15] M.E. O'Hern, C.J. McHargue, C.W. White and G.C. Farlow, Nucl. Instr. and Meth. B 46 (1990) 171.
[16] E.D. Specht, C.J. Sparks and C.J. McHargue, Appl. Phys. Lett. 60 (1992) 2216.
[17] R.A. Cowley and T.W. Ryan, J. Phys. D 20 (1987) 61.
[18] LG. Parratt, Phys. Rev. 95 (1954) 359.
[19] A. Braslau, M. Deutsch, P.S. Pershan, A.H. Weiss, J. Als-Nielsen and J. Bohr, Phys. Rev. Lett. 54 (1985) 114.
[20] M. Abramowitz and I.A. Stegun (eds.), Handbook of Mathematical Functions (Dover, New York, 1965) p. 297.
[21] D.S. Phillips, T.E. Mitchell and A.H. Heuer, Philos. Mag. A 42 (1980) 417.
[22] T. Hioki, A. Itoh, M. Ohkubo, S. Noda, H. Doi, J. Kawamoto and O. Kaigaito, J. Mater. Sci. 21 (1986) 1321.
[23] See: J.P. Biersack and L.G. Haggmark, Nucl. Instr. and Meth. 174 (1980) 257, for the original TRIM program. TRIM89 has been modified by T.P. Sjoreen (unpublished) to include different displacement thresholds for elements in compound materials.
[24] J.P. Biersack and L.G. Haggmark, Nucl. Instr. and Meth. 174 (1980) 257.
[25] G.P. Pells and D.C. Phillips, J. Nucl. Mater. 80 (1979) 207.
[26] A.E. Paladino and W.D. Kingery, J. Chem. Phys. 37 (1962) 957.
[27] Y. Oishi and W.D. Kingery, J. Chem. Phys. 33 (1960) 480.
[28] C.W. White, G.C. Farlow, C.J. McHargue, P.S. Sklad, M.P. Angelini and B.R. Appleton, Nucl. Instr. and Meth. B 7/8 (1985) 473.
[29] C.W. White, L.A. Boatner, P.S. Sklad, C.J. McHargue, J. Rnakin, G.C. Farlow and M.J. Aziz, Nucl. Instr. and Meth. B 32 (1988) 11.
[30] N. Swanson, Phys. Rev. 165 (1968) 1067.